Programmable Rainbow Trapping and Band-Gap Enhancement via Spatial Group-Velocity Tailoring in Elastic Metamaterials

Mustafa Alshaqaq[*], Christopher Sugino, and Alper Erturk

G.W. Woodruff School of Mechanical Engineering, Georgia Institute of Technology, Atlanta, Georgia 30332, USA

We numerically and experimentally investigate spatially programmable rainbow trapping and band-gap enhancement using a graded piezoelectric metamaterial beam with unit cells shunted to synthetic impedance circuits. The local inductive shunt resonant frequency of each unit cell is different and follows a predefined spatial variation along the beam length. We explore the effect of various grading profiles on the spatial wave trapping and on the attenuation bandwidth. Experiments are performed on a clamped-clamped metamaterial beam with 29 piezoelectric elements shunted to synthetic impedance circuits with gradually varying inductance. Numerical simulations and experimental results reveal that, over a frequency band containing all resonant frequencies of unit cells, propagating elastic waves can be trapped uniformly or nonuniformly along the beam, and that the spatial trapping pattern follows the respective target frequency grading profile. Additionally, substantial band-gap enhancement is observed (as high as 75% increase) as compared with the identical resonators counterpart. Overall, the results show the versatility of this class of graded piezoelectric metamaterials and support the design of such programmable piezoelectric metastructures.

The "rainbow trapping" effect is observed when waves slow down as they propagate until they stop at different spatial positions depending on their frequency, leading to a temporary trapping of waves at specific locations along a waveguide. This phenomenon has been shown in electromagnetic and plasmonic work in which propagating electromagnetic waves with different frequency components can be slowed down and trapped at different locations, allowing for storage of light at specific locations along a waveguide [1–5]. This phenomenon and resulting dynamics have inspired researchers to study and implement the rainbow trapping effect in acoustic [6–9] and elastic [10–13] waves.

Metamaterials, architected structures that derive their large-scale effective properties from the small-scale properties of their constituent unit cells, are a well-suited platform for implementing rainbow trapping. Metamaterials can exhibit exotic effective properties, such as negative effective density [14,15], negative stiffness and modulus [16,17], double-negative [18–21] properties, or "fluidlike" [22,23] properties for elastic solids. Furthermore, metamaterials can vary the local wave propagation velocity through gradual variation of the properties of their constituent unit cells. Generally, there are two widely used mechanisms to introduce such grading in metamaterials

and metastructures: (i) gradually varying a particular property of the resonating element in unit cells and (ii) using graded material contrast with different refractive index [24–28]. In a broader sense, graded locally resonant metamaterials are composed of locally resonant elements with gradually varying properties that exhibit interesting phenomena such as wave trapping, enhanced wave manipulation, and wave mode conversion [29–31], among others. In the existing literature, graded metamaterials with linearly varying unit cell properties have been given the most attention.

In this study, we explore a fully programmable piezoelectric metamaterial beam in which the graded array of piezoelectric unit cells are shunted to synthetic impedance circuits (Fig. 1). Piezoelectric metamaterials have effective mechanical properties that depend on the shunt circuit in each unit cell. More specifically, it has been shown that the effective dynamic stiffness of a piezoelectric metamaterial depends on the admittance of the shunt circuit in each unit cell [17]. Synthetic impedance [32,33] enables precise spatial programming of the impedance of each unit cell's shunt circuit, leading to the easy assignment of any grading profile to the unit cells. Specifically, the grading is performed on the resonant frequency of each unit cell by varying the inductance provided by each synthetic impedance shunt circuit. Background on synthetic impedance-based piezoelectric metamaterials [34] and graded metamaterials [35] can be found elsewhere.
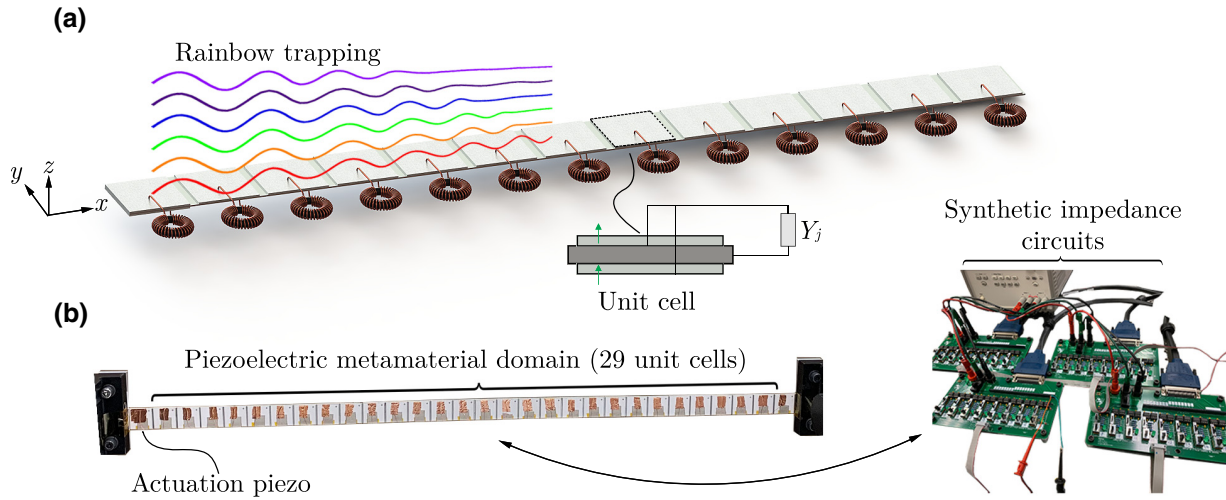
---
[*]mshaqaq3@gatech.edu

FIG. 1. (a) Schematic of the programmable piezoelectric metamaterial beam. The piezoelectric patches are connected in parallel with poling directions shown by green arrows. (b) Experimental realization of a piezoelectric metamaterial beam with 29 unit cells. The impedance across each unit cell is controlled by a synthetic circuit allowing precise control of impedance values.

We consider a piezoelectric metamaterial beam made from a 1D periodic array of unit cells, shown schematically in Fig. 1. Each unit cell comprises a pair of square piezoelectric patches (PZT-5J) with dimensions $21 \times 21 \times 0.55$ mm bonded symmetrically to a 0.51-mm-thick conductive shim (Aluminum 6061). Both piezoelectric elements in each unit cell are poled in the same direction through the thickness for parallel wiring. The system has lattice constant $a = 22$ mm, and each unit cell is numbered with index j, such that the jth unit cell is at position $x_j = ja$. The outer electrodes of each unit cell are electrically connected to a synthetic impedance circuit, which is programmed to provide a synthetic admittance corresponding to the series connection of a resistor and inductor, i.e.,

$$Y_j(s) = \frac{1}{R_j + L_j s}, \qquad (1)$$

where R_j and L_j are the jth circuit resistance and inductance, respectively, and s is the complex Laplace variable. Each shunt admittance is normalized by the piezoelectric capacitance of that unit cell, yielding

$$h_j(s) = \frac{Y_j(s)}{C_{p,j}} = \frac{\omega_{t,j}^2}{s + 2\zeta_j \omega_{t,j}}, \qquad (2)$$

where $\omega_{t,j} = 1/\sqrt{C_{p,j} L_j}$ is the resonant frequency of the jth shunt circuit and $\zeta_j = (R_j/2)\sqrt{C_{p,j}/L_j}$ is its damping ratio. In practice, it is necessary to add a bias resistance R_b in parallel to the synthetic impedance shunt to dissipate dc bias current. Additionally, the damping ratio ζ_j in this work is selected to be as small as possible while maintaining the stability of the system. In the numerical results, both the bias resistance R_b and series resistance R_j are neglected to highlight the rainbow trapping phenomenon.

We consider a frequency grading pattern for the shunt circuits given by

$$\omega_{t,j} = \left[1 + \delta - 2\delta \left(\frac{j-1}{S-1} \right)^p \right] \omega_t, \qquad (3)$$

where $\omega_{t,j}$ is the target frequency of the jth unit cell, S is the total number of unit cells in the structure, ω_t is some target frequency around which gradual variation of the shunt circuit frequencies take place, the dimensionless parameter δ quantifies the variations of shunt circuit frequencies from the target one, and the power p defines the profile of the frequency grading between the first and the last shunt circuits.

To quantify the effect of each shunt circuit on the metamaterial, we consider a finite-element model (COMSOL Multiphysics) of the system's unit cell. The unit cell is characterized by its dispersion, which describes the relation between the velocity and frequency of a wave propagating through the metamaterial. Dispersion curves are computed by imposing Floquet boundary conditions with wave number k and calculating the corresponding eigenfrequencies $\omega(k)$; the group velocity can then be calculated as $d\omega/dk$. Near the target frequency of the shunt the dispersion curve bends sharply, allowing the group velocity to be tuned at a given frequency. By varying the target frequency in space, the group velocity at a given frequency also varies in space. This calculation procedure is shown schematically in Fig. 2.

For each target frequency profile given by Eq. (3), the corresponding group velocity can be computed as a
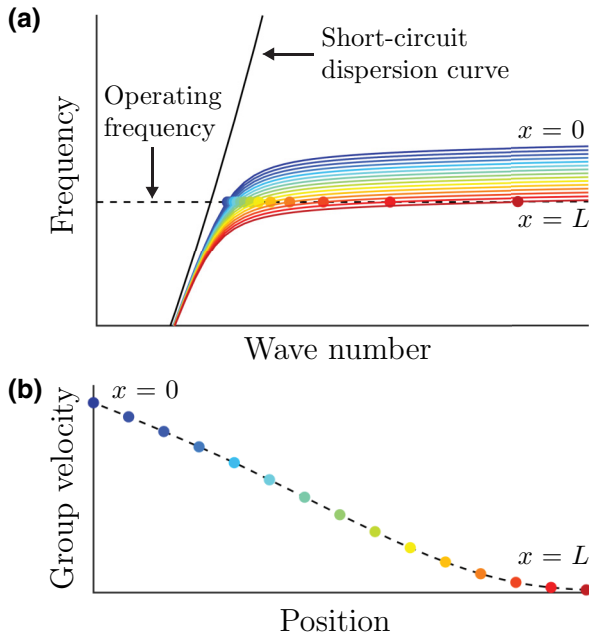
FIG. 2. (a) Example dispersion curve at short circuit (black solid line) and dispersion curves with linear spatial variation in the target frequency $\omega_{t,j}$ (colored lines). At a certain operating frequency (dashed line), the intersection with the dispersion curves (solid markers) varies in wave number. (b) Group velocity versus position corresponding to (a) at the shown operating frequency.
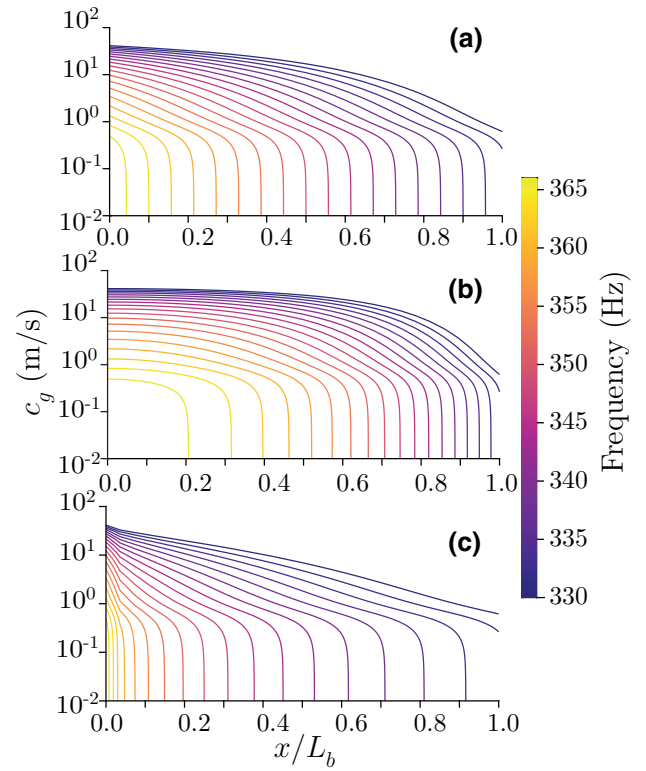

FIG. 3. Group velocity versus beam length for different grading profiles with $\delta = 0.05$ and (a) $p = 1$, (b) $p = 2$, and (c) $p = 1/2$. The panels clearly show the cutoff position where the group velocity becomes zero. Uniform spacing of the zero group velocity points is observed when the grading profile is linear (a), whereas nonuniform spacing is observed for (b) $p = 2$ and (c) $p = 0.5$.

function of frequency and position to demonstrate the rainbow trapping phenomenon, in which waves of different frequencies slowed down and stopped at different positions. This is shown in Fig. 3 for grading profiles with $\omega_t/(2\pi) = 350$ Hz, $\delta = 0.05$, and $p = 0.5, 1, 2$, with no loss in the system. It is observed that the group velocity becomes zero at different spatial points depending on the considered grading profile. Figure 3(a) shows uniform trapping of waves (uniform zero group velocity points) along the beam over a frequency range bounded by the lowest and highest frequency grading of unit cells. When the grading profile is quadratic ($p = 2$) as shown in Fig. 3(b), the zero group velocity points are concentrated at the far end of the beam away from the excitation unit cell. On the other hand, when a fractional grading profile ($p = 1/2$) is considered, the zero group velocity points are concentrated in a region near the excitation unit cell as shown in Fig. 3(c). In all cases, the grading profile determines at which points the elastic waves stop propagating. A propagating wave with a frequency of 350 Hz under a linear grading profile will eventually stop at the center of the beam. However, the same wave under a fractional grading profile will be trapped in a region smaller than half the beam.

Experiments are performed to validate the rainbow trapping predictions of Fig. 3 using a piezoelectric metamaterial beam. The experimental setup consists of a clamped-clamped beam comprising 30 piezoelectric unit cells described previously (Fig. 1), with total length $L_b = 660$ mm. The system is excited by applying a white noise burst to the piezoelectric unit cell closest to one clamped end of the beam, while the remaining 29 unit cells are connected to synthetic impedance circuits operating at 400-kHz sampling frequency. The transmissibility frequency response functions (FRFs) between the measured velocity of the first unit cell and the velocities of 127 measurement points distributed along the beam length are measured using a Polytec PSV-500 scanning laser Doppler vibrometer. The numerical results of Fig. 3 rely on unit cell dispersion properties, and hence do not take into account the finite size of the experimental setup. Thus, numerical simulations are performed using a finite-element model of the full structure to compare directly with the experimental results. In the finite-element model of the full system, an isotropic loss factor of 0.001 is used to highlight the rainbow trapping effect in the numerical results.

Figures [4(a)]–[4(c)] show the numerical transmissibility FRF versus the excitation frequency and position for different grading profiles p when the variation parameter δ is 0.05. As shown in the figures, the target frequency profiles associated with unit cells control the trend of vibration attenuation along the beam. That is, when the grading profile is linear, $p = 1$, the band gap forms uniformly along the beam with respect to the excitation frequency while for the other grading profiles, $p = 2$ and $p = 1/2$, band gaps open nonuniformly [37]. These numerical observations are in agreement with the group velocity plots in Fig. [3] in which zero group velocity of waves with different frequencies occurs at different positions. This confirms that the opening of band gaps follows in shape the frequency grading profile of unit cells. Figures [4(d)]–[4(f)] show the corresponding experimental transmissibility colormaps, which agree well with the numerical ones. It can be observed that the experimental transmissibility displays the same frequency-dependent attenuation, with the band-gap cutoff closely following the prescribed profile. However, the mechanical damping in the experimental system is significantly larger than in the simulations, and so the attenuation

FIG. 5. (a) Numerical simulations and (b) experimental results demonstrating the rainbow trapping of elastic waves. The left-hand panels show the transmissibility colormaps of the graded metamaterial beam with $p = 2$ and $\delta = 0.05$. The right-hand panels show the wave profiles at different excitation frequencies between 340 and 365 Hz inside the band gap.

inside the band gap is less extreme. Similarly, the vibrational modes of the metamaterial are less pronounced in the experimental data than in the numerical simulations.

To highlight the rainbow trapping effect, Figs. [5(a)] and [5(b)] show the numerical and experimental steady-state wave profiles at several excitation frequencies inside the band gap for a second-order grading profile ($p = 2$) with $\delta = 0.05$. The wave profile at a frequency corresponding to the start of the band gap (the lowest frequency) propagates throughout the length of the beam. As the excitation frequency increases, the waves are trapped gradually at specific regions along the beam, which demonstrates the rainbow trapping phenomenon. Again, there is excellent agreement between the numerical and experimental results.

Finally, to determine the effect of the grading profile on band-gap size, we consider the transmissibility of the metamaterial averaged over five points near the clamped end farthest from the excitation point. Figure [6] shows averaged transmissibility FRFs for different levels of the variation parameter δ and three levels of the grading power $p = 1$,
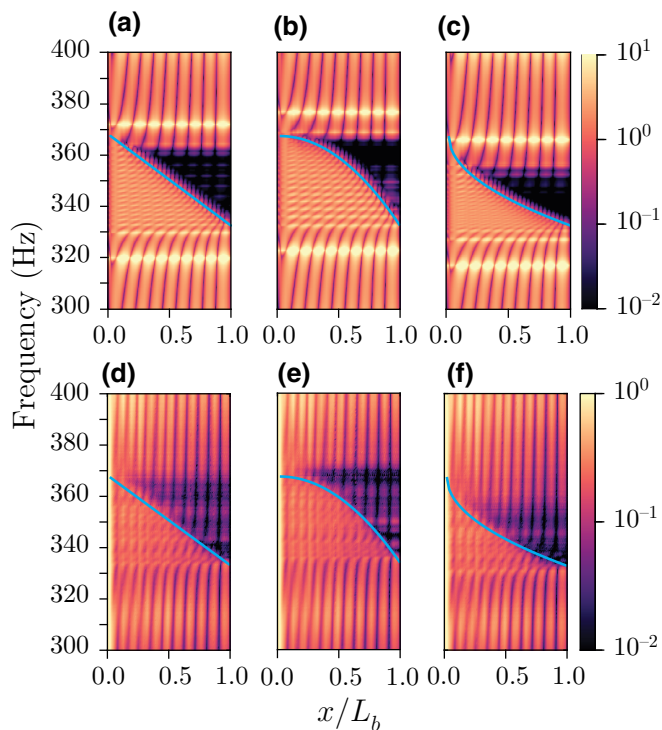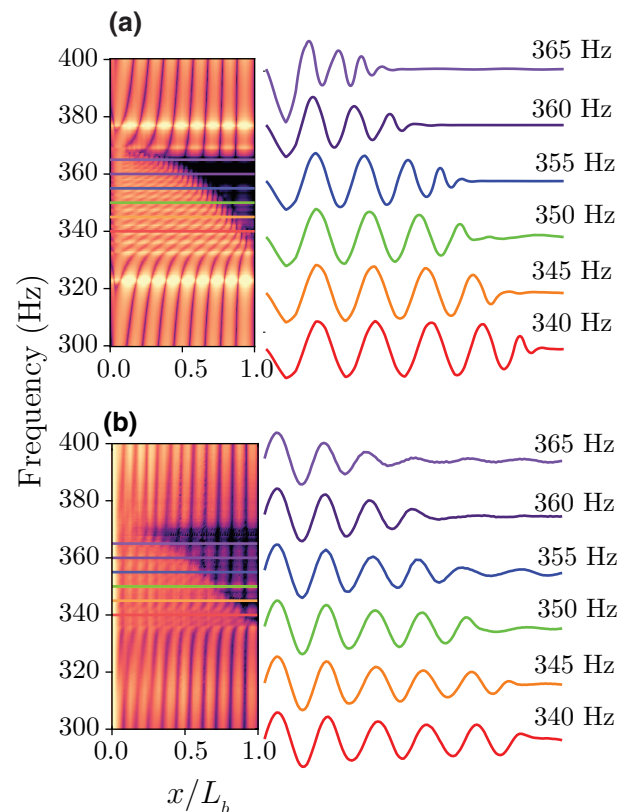

FIG. 4. Numerical and experimental transmissibility colormaps versus the excitation frequency and the beam length for different grading profiles shown by the blue line in each colormap for $\delta = 0.05$ (light damping is assumed in the numerical simulations). (a)–(c) The numerical simulations and (d)–(f) the experimental results (each row with the same order: $p = 1$, $p = 2$, and $p = 1/2$). See the Supplemental Material [36] for an animation of the colormaps for different δ values.
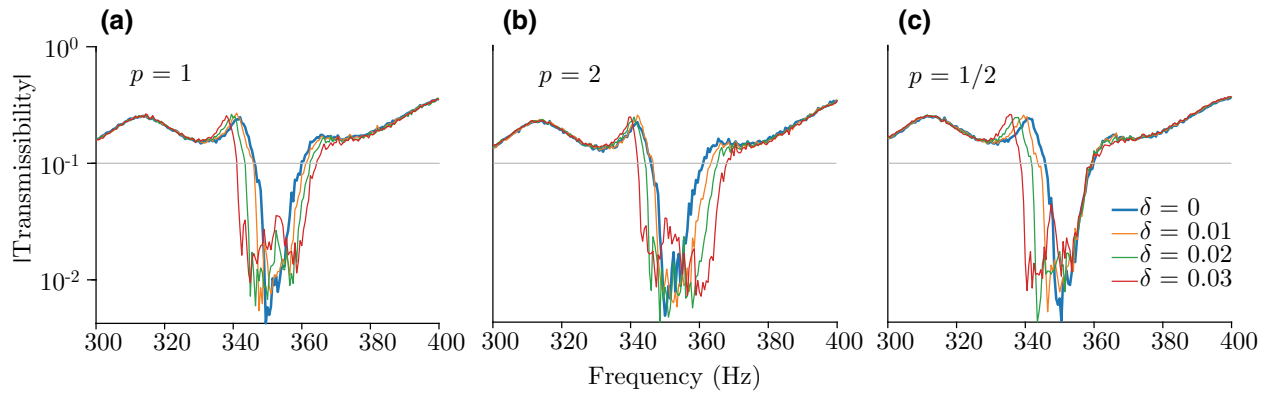
FIG. 6. Experimental transmissibility plots for (a) $p = 1$, (b) $p = 2$, and (c) $p = 1/2$ profiles at different levels of the variation parameter δ showing increase in the band-gap width.

$p = 2$, and $p = 1/2$. The figure shows that, as the variation parameter δ increases, the band gap becomes wider but the attenuation inside the band gap becomes weaker. Here, the band-gap width is measured for transmissibility below 0.1. The corresponding percentage increase in the band-gap width for each case is tabulated in Table I as compared to the corresponding band gap in the uniform (identical) resonators counterpart [17,34].

In conclusion, we demonstrate the rainbow trapping effect using a fully programmable elastic metamaterial beam with unit cells shunted to synthetic impedance circuits. This system allows us to freely control the grading profile of unit cells by digitally tuning the respective inductance values in the synthetic impedance circuits. Various grading profiles are numerically and experimentally investigated to reveal the corresponding trapping characteristics. First-order grading profiles show uniform trapping of elastic waves such that the trapping width along the beam decreases linearly with the increase in the excitation frequency. On the other hand, quadratic and fractional grading profiles exhibit spatially nonuniform trapping. Moreover, the results show that the increase in the band-gap width depends significantly on the variation parameter and to a lesser degree on the profile shape. The results reveal the significance of this class of programmable metamaterials to achieve precise control of elastic wave trapping, spatial filtering, and attenuation. For example, a programmable metamaterial could use the rainbow trapping effect to sense and physically separate incident elastic

waves over a wide frequency range, or to provide reconfigurable broadband wave and vibration attenuation. Future work could also explore time-varying versions of the rainbow trapping phenomenon leveraging the programmable nature of synthetic impedance circuits.

[1] K. L. Tsakmakidis, A. D. Boardman, and O. Hess, 'Trapped rainbow' storage of light in metamaterials, Nature **450**, 397 (2007).

[2] Q. Gan, Y. Gao, K. Wagner, D. Vezenov, Y. J. Ding, and F. J. Bartoli, Experimental verification of the rainbow trapping effect in adiabatic plasmonic gratings, Proc. National Acad. Sci. **108**, 5169 (2011).

[3] M. S. Jang and H. Atwater, Plasmonic Rainbow Trapping Structures for Light Localization and Spectrum Splitting, Phys. Rev. Lett. **107**, 207401 (2011).

[4] H. Hu, D. Ji, X. Zeng, K. Liu, and Q. Gan, Rainbow trapping in hyperbolic metamaterial waveguide, Sci. Rep. **3**, 1 (2013).

[5] Z. Xu, J. Shi, R. J. Davis, X. Yin, and D. F. Sievenpiper, Rainbow Trapping with Long Oscillation Lifetimes in Gradient Magnetoinductive Metasurfaces, Phys. Rev. Appl. **12**, 024043 (2019).

[6] J. Zhu, Y. Chen, X. Zhu, F. J. Garcia-Vidal, X. Yin, W. Zhang, and X. Zhang, Acoustic rainbow trapping, Sci. Rep. **3**, 1728 (2013).

[7] X. Ni, Y. Wu, Z.-G. Chen, L.-Y. Zheng, Y.-L. Xu, P. Nayar, X.-P. Liu, M.-H. Lu, and Y.-F. Chen, Acoustic rainbow trapping by coiling up space, Sci. Rep. **4**, 1 (2014).

[8] C. Zhou, B. Yuan, Y. Cheng, and X. Liu, Precise rainbow trapping for low-frequency acoustic waves with micro mie resonance-based structures, Appl. Phys. Lett. **108**, 063501 (2016).

[9] L. Zhao and S. Zhou, Compact acoustic rainbow trapping in a bioinspired spiral array of graded locally resonant metamaterials, Sensors **19**, 788 (2019).

[10] D. Cardella, P. Celli, and S. Gonella, Manipulating waves by distilling frequencies: A tunable shunt-enabled rainbow trap, Smart Mater. Struct. **25**, 085017 (2016).

TABLE I. Percent increase in band-gap width for different grading profiles at different levels of variation parameter (compared with identical resonators case).

	$\delta = 0.01$	$\delta = 0.02$	$\delta = 0.03$
$p = 1$	10.7%	35.7%	60.7%
$p = 2$	10.7%	39.3%	75.0%
$p = 1/2$	14.3%	21.4%	50.0%

[11] J. M. De Ponti, A. Colombi, R. Ardito, F. Braghin, A. Corigliano, and R. V. Craster, Graded elastic metasurface for enhanced energy harvesting, New J. Phys. **22**, 013013 (2020).

[12] J. M. De Ponti, A. Colombi, E. Riva, R. Ardito, F. Braghin, A. Corigliano, and R. V. Craster, Experimental investigation of amplification, via a mechanical delay-line, in a rainbow-based metamaterial for energy harvesting, Appl. Phys. Lett. **117**, 143902 (2020).

[13] G. J. Chaplain, J. M. De Ponti, G. Aguzzi, A. Colombi, and R. V. Craster, Topological Rainbow Trapping for Elastic Energy Harvesting in Graded Su-Schrieffer-Heeger Systems, Phys. Rev. Appl. **14**, 054035 (2020).

[14] Z. Liu, X. Zhang, Y. Mao, Y. Zhu, Z. Yang, C. T. Chan, and P. Sheng, Locally resonant sonic materials, Science **289**, 1734 (2000).

[15] Z. Yang, J. Mei, M. Yang, N. Chan, and P. Sheng, Membrane-Type Acoustic Metamaterial with Negative Dynamic Mass, Phys. Rev. Lett. **101**, 204301 (2008).

[16] N. Fang, D. Xi, J. Xu, M. Ambati, W. Srituravanich, C. Sun, and X. Zhang, Ultrasonic metamaterials with negative modulus, Nat. Mater. **5**, 452 (2006).

[17] C. Sugino, S. Leadenham, M. Ruzzene, and A. Erturk, An investigation of electroelastic bandgap formation in locally resonant piezoelectric metastructures, Smart Mater. Struct. **26**, 055029 (2017).

[18] J. Li and C. T. Chan, Double-negative acoustic material, Phys. Rev. E **70**, 055602 (2004).

[19] Y. Ding, Z. Liu, C. Qiu, and J. Shi, Metamaterial with Simultaneously Negative Bulk Modulus and Mass Density, Phys. Rev. Lett. **99**, 093904 (2007).

[20] Y. Wu, Y. Lai, and Z.-Q. Zhang, Elastic Metamaterials with Simultaneously Negative Effective Shear Modulus and Mass Density, Phys. Rev. Lett. **107**, 105506 (2011).

[21] J. Shi, C. Liu, and Y. Lai, Controlling the effective bending stiffness via out-of-plane rotational resonances in elastic metamaterial thin plates, New J. Phys. **20**, 103043 (2018).

[22] Y. Lai, Y. Wu, P. Sheng, and Z.-Q. Zhang, Hybrid elastic solids, Nat. Mater. **10**, 620 (2011).

[23] G. Ma, C. Fu, G. Wang, P. Del Hougne, J. Christensen, Y. Lai, and P. Sheng, Polarization bandgaps and fluid-like elasticity in fully solid elastic metamaterials, Nat. Commun. **7**, 1 (2016).

[24] S.-C. S. Lin, T. J. Huang, J.-H. Sun, and T.-T. Wu, Gradient-index phononic crystals, Phys. Rev. B **79**, 094302 (2009).

[25] X. Yan, R. Zhu, G. Huang, and F.-G. Yuan, Focusing guided waves using surface bonded elastic metamaterials, Appl. Phys. Lett. **103**, 121901 (2013).

[26] Y. Jin, D. Torrent, Y. Pennec, Y. Pan, and B. Djafari-Rouhani, Simultaneous control of the s0 and a0 lamb modes by graded phononic crystal plates, J. Appl. Phys. **117**, 244904 (2015).

[27] J. Zhao, B. Li, Z. Chen, and C.-W. Qiu, Manipulating acoustic wavefront by inhomogeneous impedance and steerable extraordinary reflection, Sci. Rep. **3**, 1 (2013).

[28] S. Tol, F. Degertekin, and A. Erturk, Phononic crystal luneburg lens for omnidirectional elastic wave focusing and energy harvesting, Appl. Phys. Lett. **111**, 013503 (2017).

[29] A. Colombi, D. Colquitt, P. Roux, S. Guenneau, and R. V. Craster, A seismic metamaterial: The resonant metawedge, Sci. Rep. **6**, 1 (2016).

[30] A. Colombi, R. V. Craster, D. Colquitt, Y. Achaoui, S. Guenneau, P. Roux, and M. Rupin, Elastic wave control beyond band-gaps: Shaping the flow of waves in plates and half-spaces with subwavelength resonant rods, Front. Mech. Eng. **3**, 10 (2017).

[31] S. Alan, A. Allam, and A. Erturk, Programmable mode conversion and bandgap formation for surface acoustic waves using piezoelectric metamaterials, Appl. Phys. Lett. **115**, 093502 (2019).

[32] A. Fleming, S. Behrens, and S. Moheimani, Synthetic impedance for implementation of piezoelectric shunt-damping circuits, Electron. Lett. **36**, 1525 (2000).

[33] J. Nečásek, J. Václavík, and P. Márton, Digital synthetic impedance for application in vibration damping, Rev. Sci. Instrum. **87**, 024704 (2016).

[34] C. Sugino, M. Ruzzene, and A. Erturk, Digitally Programmable Resonant Elastic Metamaterials, Phys. Rev. Appl. **13**, 061001 (2020).

[35] M. Alshaqaq and A. Erturk, Graded multifunctional piezoelectric metastructures for wideband vibration attenuation and energy harvesting, Smart Mater. Struct. **30**, 015029 (2020).

[36] See Supplemental Material at http://link.aps.org/supplemental/10.1103/PhysRevApplied.17.L021003 for an animation of the colormaps for different δ values.

[37] Note that the target frequency being at the lower or upper boundary of the band gap depends on the capacitance value being used in the simulation; cf. Ref. [35] theory and simulations—likewise cf. Refs. [17] and [34].